

# The $\mathbb{R}P^2$ Valued Sigma and Baby Skyrme Models

Matthew D E Szyndel<sup>1</sup>

Centre for Particle Theory,  
 Mathematical Sciences,  
 University of Durham,  
 Durham,  
 DH1 3LE,  
 UK.

## Abstract

We investigate the sigma and baby Skyrme models with an  $\mathbb{R}P^2$  target space. We compare these models to models with an  $S^2$  target space. We investigate the interactions between solitons and defects in the  $\mathbb{R}P^2$  sigma model.

## 1 Introduction

The Skyrme model has long been of interest as an effective field theory of nucleons [1]. The 2 dimensional baby Skyrme model allows us to study a more tractable analogue of the Skyrme model [2]. The related O(3) sigma model is applicable to some condensed matter systems. Nematic liquid crystals are a condensed matter system where the target space is not  $S^2$  but  $\mathbb{R}P^2$ . In this paper we describe our work on the variants of the baby Skyrme model and O(3) sigma model using  $\mathbb{R}P^2$  as a target space.

### 1.1 Models

The O(3) sigma model describes maps from  $\mathbb{R}^2$  (the “physical” space) to  $S^2$  (the “target” space).  $\mathbb{R}^2$  is the normal Euclidean plane, whereas  $S^2$  is the 2 dimensional surface of a unit sphere embedded in 3 Euclidean dimensions. The lagragian of the O(3) sigma model is given by

$$\mathcal{L} = \frac{1}{4} \partial^\mu \vec{\phi} \cdot \partial_\mu \vec{\phi}, \quad (1)$$

---

<sup>1</sup>email: m.d.e.szyndel@durham.ac.uk

where  $\vec{\phi} \in \mathbb{R}^3$  such that  $\vec{\phi} \cdot \vec{\phi} = 1$ . The condition that  $\vec{\phi} \mapsto \vec{\phi}_{vac}$  as  $r \mapsto \infty$ , where  $r$  is spatial radius, is usually imposed to keep the action finite. This effectively compactifies the physical space from  $\mathbb{R}^2$  to  $S^2$ . This in turn implies that the configurations  $\vec{\phi}$  must fall into disjoint classes characterised by the elements of the second homotopy group  $\pi_2(S^2) \cong \mathbb{Z}$ . Field configurations which fall into any of the classes corresponding to non-trivial elements of  $\pi_2(S^2)$  describe ‘lumps’ of energy. These lumps are not stable, and as a result are not true solitons. This instability is due to the conformal invariance of the model – the lumps have no intrinsic scale, and so may change scale without any energetic penalty. This scale invariance may be removed by the addition of new terms to the Lagrangian, as seen below.

The first model we examined was the baby Skyrme model with the so called ‘new’ potential term. The Lagrangian is

$$\mathcal{L} = \frac{1}{4} \partial^\mu \vec{\phi} \cdot \partial_\mu \vec{\phi} + \theta_1 \frac{1}{4} ((\partial^\mu \vec{\phi} \cdot \partial^\nu \vec{\phi})(\partial_\mu \vec{\phi} \cdot \partial_\nu \vec{\phi}) - (\partial^\mu \vec{\phi} \cdot \partial_\mu \vec{\phi})^2) + \theta_2 \mathcal{L}_V, \quad (2)$$

where  $\theta_1$  and  $\theta_2$  are real positive constants. The term containing  $\theta_1$  is the so called (2 dimensional) Skyrme term. This term tends to cause solitons to broaden, and is the only possible Lorentz covariant term of fourth order with only first order time derivatives. The term containing  $\theta_2$  is normally referred to as the potential term. This term is chosen so that it acts to shrink the size of the soliton. Consequently a stable equilibrium may be reached where the effects of the Skyrme term and potential term balance. A number of different potential terms have been studied [2, 3], but our  $\mathbb{R}P^2$  target space forces us to use a potential term which is invariant under the transformation  $\vec{\phi} \mapsto -\vec{\phi}$ . A good choice would be the so called ‘new’ potential

$$\mathcal{L}_V = \frac{1}{4} (1 - (\vec{\phi} \cdot \vec{\phi}_{vac})^2). \quad (3)$$

## 1.2 The Geometry and Topology of $\mathbb{R}P^2$

### 1.2.1 Geometry

$\mathbb{R}P^2$  may be thought of as a hemisphere, and so may be parameterised by a unit 3-vector  $\vec{\phi}$  where  $\vec{\phi}(x) \equiv -\vec{\phi}(x)$ .  $\mathbb{R}P^2$  may also be described locally by a 2-vector  $\vec{\chi}$  where

$$\chi_j^i = \frac{\phi_j}{\phi_i} \quad i = 1..3 \quad j = 1..3.$$

Here  $i$  labels which chart is being used, and  $j$  labels the components of  $\vec{\chi}$ .  $\vec{\chi}$  appears to have 3 components in this definition but, as the component  $\chi_i^i$  is always 1,  $\vec{\chi}$  has only 2 degrees of freedom. The chart labeled  $i$  is ill defined on the equator  $\phi_i = 0$ , and so all three charts are required to cover  $\mathbb{R}P^2$  – the first covers all of the manifold except for an equator, the second all of this equator except for 2 antipodal points and the third those two points.

A neat way to combine all three  $\vec{\chi}$  charts is to use the matrix  $P_{ij}(x) = \phi_i(x)\phi_j(x)$ . Each chart is easily extracted as  $\chi_j^i = \frac{P_{ij}}{P_{ii}}$  with no sum implied by repeated indices.

### 1.2.2 Topology

The  $n$ th homotopy group of  $\mathbb{R}P^2$  can be found quickly for  $n \geq 2$  as  $S^2$  is a universal covering space of  $\mathbb{R}P^2$ . A theorem found in [4] states that this implies that  $\pi_n(S^2) \cong \pi_n(\mathbb{R}P^2) \quad \forall \quad n \geq 2$ .  $\pi_1(\mathbb{R}P^2)$  may be found to be the second symmetric group,  $\mathbb{Z}_2$ . To summarise:

$$\pi_1(S^2) \cong e \quad \pi_1(\mathbb{R}P^2) \cong \mathbb{Z}_2, \quad (4)$$

$$\pi_2(S^2) \cong \mathbb{Z} \quad \pi_2(\mathbb{R}P^2) \cong \mathbb{Z}, \quad (5)$$

$$\pi_3(S^2) \cong \mathbb{Z} \quad \pi_3(\mathbb{R}P^2) \cong \mathbb{Z}, \quad (6)$$

### 1.2.3 Winding Number

The class of field configuration  $\vec{\phi}$  may be characterised by the degree of map, or winding number. To calculate the winding number we must calculate the pullback of the two form on the target space; the map  $\vec{\phi}$  from the physical space to the target space induces a natural map (the ‘‘pullback’’) from the two form on the target space to a two form on the physical space. If the two form on the physical space is then integrated over all space the result must be a multiple of an integer. By renormalising we get a formula for the integer valued winding number:

$$T = \frac{1}{8\pi} \int d^2x \epsilon_{ij} \epsilon_{abc} \phi_a (\partial_i \phi_b) (\partial_j \phi_c). \quad (7)$$

It should be noted that the transformation  $\vec{\phi} \mapsto -\vec{\phi}$  leads to  $T \mapsto -T$ . This is because  $\mathbb{R}P^2$  is a non-orientable manifold – a two form is not well defined on  $\mathbb{R}P^2$  as its sense is changed by a translation along a non-trivial loop. In fact it may be shown [5] that field configurations of  $\vec{\phi}$  are characterised not by  $\pi_2(\mathcal{M})$  but by  $\pi_2(\mathcal{M})/\pi_1(\mathcal{M})$ . In the case of an  $\mathbb{R}P^2$  target space this means that field configurations are characterised by  $\mathbb{Z}/\mathbb{Z}_2$ .

## 1.3 Numerical Techniques

The models outlined above are highly nonlinear and more or less completely intractable analytically. The models are, however, open to study using numerical techniques. One may write a simulation on a discrete grid and analyse the evolution of an arbitrary initial state. With a clever ansatz for the initial conditions, with or without the use of a relaxation routine, the behaviour of minimal energy field configurations may be studied.

We simulated the sigma and Skyrme models numerically, using  $\mathbb{R}P^2$  as the target space. Our simulations were based on a  $200 \times 200$  point grid using the

nine point laplacian and derivatives outlined in [6], together with a fourth order Runge-Kutta algorithm for simulating time evolution. The timestep length was set to half the gridpoint spacing. To give the  $\mathbb{R}P^2$  topology the state vector was stored using the  $P$  matrix described in section (1.2.1) for position on the target space, and  $Q_{ij} = \dot{P}_{ij} = \phi_i \dot{\phi}_j + \dot{\phi}_i \phi_j$  for the rate of change of position on the target space with time, where a dot is used to denote derivatives with respect to time. The simulation then evaluated derivatives by determining the field as the equivalent  $\vec{\phi}$  for any given set of nine points, with the central point mapped to the north pole of  $S^2$ . Reflections from the boundaries of the grid were reduced by damping out kinetic energy in a region near the boundary. The fields were kept on manifold by applying the following transformations each timestep:

$$P'_{ij} = \frac{P_{ij}}{P_{kk}}, \quad (8)$$

$$Q'_{ij} = \frac{Q_{ij} - P'_{ij} Q_{kk}}{\sqrt{P_{kk}}}. \quad (9)$$

These transformations ensure that  $Tr(P) = 1$  (i.e. the field lies on  $\mathbb{R}P^2$ ) and that  $Tr(Q) = 0$  (i.e. the rate of change of the field is tangential to the surface of the field manifold).

## 2 The $\mathbb{R}P^2$ Valued New Baby Skyrme Model

Simulations of this model were in close qualitative and quantitative agreement with simulations using an  $S^2$  target space.

### 2.1 The Hedgehog Anzatz

As in the  $S^2$  model the simplest ansatz for a skyrmion is the radially symmetric ansatz, usually referred to as the ‘hedgehog’ ansatz [3]. For a skyrmion of topological charge one this ansatz gives:

$$\vec{\phi} = \begin{pmatrix} \sin[f(r)] \cos(\theta - \gamma) \\ \sin[f(r)] \sin(\theta - \gamma) \\ \cos[f(r)] \end{pmatrix}. \quad (10)$$

Here  $f(r)$  is known as the profile function and  $\gamma$  is an arbitrary phase parameter. This profile function is arbitrary up to the boundary condition that  $f(0) = (2n + 1)\pi$  and  $f(\infty) = 2m\pi$  where  $n, m \in \mathbb{Z}$ . To minimise the energy of the ansatz one may determine the energy of the field as a functional of the profile function and its first derivative, as shown below:

$$E = 2\pi \int_0^\infty r dr (f'^2 + \frac{\sin^2 f}{r^2} (1 + 2\theta_1 f'^2) + \theta_2 V(f)). \quad (11)$$

One may then use the calculus of variations to extremise this energy with the appropriate limits at  $r = 0$  and  $r = \infty$ . The resulting Euler-Lagrange equation is a non linear second order ODE for the profile function. We solved this

numerically, using the shooting method. This ansatz leads to a stable single skyrmion. Note that our ansatz is identical to that of the  $S^2$  skyrmion, and so our result agrees with the result of Weidig [3]. Simulations showed this ansatz to be stable, again in agreement with Weidig. Note that the energy has been defined such that the energy of a hedgehog ansatz soliton with  $\theta_1 = \theta_2 = 0$  is given by  $E = 1$ .

## 2.2 Two Skyrmions

As for the  $S^2$  model, a two skyrmion ansatz may be arrived at by taking the stereographic projection from the north pole of a one skyrmion:

$$W = \frac{\phi_1 + i\phi_2}{1 - \phi_3}. \quad (12)$$

This may then be combined with another skyrmion using the ansatz

$$\frac{1}{W_T} = \frac{1}{W_1} + \frac{1}{W_2}, \quad (13)$$

so that the final field  $W_T$  is approximately equal to the field for any skyrmion near that skyrmion (where  $W = 0$ ) and the final field takes the vacuum value of  $W = \infty$  at spatial infinity. Using this ansatz we were able to reproduce the attractive and repulsive channels found in [3], as well as the ninety degree scattering found in the attractive channel.

## 2.3 Equivalence of $S^2$ and $\mathbb{R}P^2$ models for Smooth Maps

In fact the two models are exactly equivalent as may be seen from the following argument. Consider maps  $f, \phi$ :

$$f : I^n \mapsto S^m, \quad (14)$$

where  $n < m$ , and

$$\phi : S^m \mapsto M. \quad (15)$$

As  $\pi_n(S^m) \cong e \quad \forall n < m$   $f$  may always be smoothly deformed to map all of  $I^n$  to a point. This implies that, for all smooth maps  $\phi$ , all  $n$ -loops in  $S^m$  shall be the pre-image of an  $n$ -loop in  $M$  corresponding to the identity element of  $\pi_n(M)$ .

One consequence of this is that for  $M \cong \mathbb{R}P^2$ ,  $n = 1$  and  $m = 2$ , all maps  $\phi$  may be described as maps to  $M \cong S^2$ , as  $\mathbb{R}P^2$  is universally covered by  $S^2$ , so the  $\mathbb{R}P^2$  new baby Skyrme model is identical to the  $S^2$  baby Skyrme model if  $\vec{\phi}$  is well defined at all points.

It is also worthy of note that this argument suggests that simulations of Fadeev-Hopf solitons [7, 8] using  $\mathbb{R}P^2$  as a target space should reproduce the simulation of such solitons with an  $S^2$  target space unless defects are present.

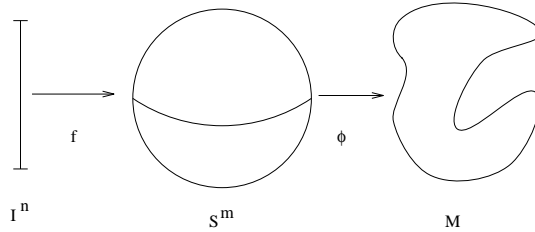


Figure 1: Maps from  $I_n$  to  $S_m$  to  $M$

### 3 The Sigma Model with Defects

The implication of the argument put forward above is that to discover new behaviour in an  $\mathbb{R}P^2$  model we must introduce a discontinuity into the field. For such a point to be stable a circle around the discontinuity in physical space must map to a non-trivial loop in the target space. If this is not the case then the discontinuity can be removed by a continuous variation in the field. These (point) discontinuities are analogous to disclination lines in a liquid crystal. We shall refer to them as “defects”. One consequence of having an odd number of defects in the system is that a contour around the edge of the physical space must map to a non-trivial loop on  $\mathbb{R}P^2$ . This means that it is no longer possible to have the field tend to a single value at spatial infinity. As a result, it is no longer easy to use a conventional potential term such as (3) in the Lagrangian. We may use the  $\mathbb{R}P^2$  sigma model, so our model has neither Skyrme nor a potential terms, or we may use an unconventional potential term. One possible potential term would be of the form

$$\mathcal{L}_V = \frac{1}{4}(\vec{\phi} \cdot \vec{\phi}_{mass})^2, \quad (16)$$

which we shall call the “easy plane” potential. This effectively gives a mass to one of the fields ( $\phi_{mass}$ ) where the potential (3) gives mass to both fields orthogonal to  $\phi_{vac}$ . Easy plane baby skyrmions have not previously been studied and so are worthy of attention in their own right. We have confined our work to the sigma model in all that follows.

It should be noted that if there is no single value for the field at infinity we are no longer compactifying the physical space to  $S^2$ . As a result winding number is no longer necessarily conserved. In fact, the physical space is topologically  $S^1 \times \mathbb{R}^1$  as not only is the space not compactified at infinity, it also has no well defined map at the point of the defect. Whilst the mapping from the target space is frozen at infinity, it is not frozen around the defect. The circle around the defect necessarily maps to a non-trivial curve in  $\mathbb{R}P^2$ . If we represent  $\mathbb{R}P^2$  as a sphere, where antipodal identification is allowed, a non-trivial curve is a line between a pair of (arbitrary) poles. If we have a defect-soliton system, one of these curves represents both the image of a circle at infinity in the physical

space, and the image of an infinitesimal circle around the defect. As a circle is contracted in from infinity to the defect, the image curve rotates around the sphere, hinged on the polar identification, wrapping the sphere once. As the image of the infinitesimal circle around the defect is able to move, it may rotate around the identified poles, unwinding the soliton like object.

We decided to study the behaviour of a soliton like lump in the presence of a point defect. To do this we need an ansatz for a soliton-defect system to use as an initial condition for our simulation. Such an ansatz needs to be sufficiently close to equilibrium to avoid large quantities of radiation perturbing the system – if the system is far from equilibrium much of the excess energy will be shed from the solitonic objects as radiation.

### 3.1 Defect Ansatz

The most obvious ansatz for a defect is a radially symmetric, planar field. A defect at  $r = 0$  may be written in polar coordinates as

$$\vec{\phi} = \begin{pmatrix} \sin \frac{\theta}{2} \\ 0 \\ \cos \frac{\theta}{2} \end{pmatrix}, \quad (17)$$

which, using the stereographic projection from the south pole,

$$W = \frac{\phi_1 + i\phi_2}{1 + \phi_3}, \quad (18)$$

is given by:

$$W = \tan \frac{\theta}{4}. \quad (19)$$

This ansatz is defined for  $0 \leq \theta < 2\pi$ . On the line  $\theta = 0$  there appears, at a first glance, to be a discontinuity in the field, but as  $\vec{\phi}$  is identified with  $-\vec{\phi}$  there is no such discontinuity. In fact any field configuration which contains a defect must have a line from the defect to infinity along which the identification between  $\vec{\phi}$  and  $-\vec{\phi}$  is made. It is simple to show analytically that the above field configuration is in equilibrium. Simulations also show that this field configuration is stable. It should be noted that this field configuration has an infinite action arising from a logarithmic divergence as  $r$  tends to infinity or as  $r$  tends to zero. This is not a problem if the physical system we are modeling is a liquid crystal. This is because such a system is, firstly, finite in extent, and, secondly, a discrete system. The field approximation is clearly not appropriate at  $r = 0$ . Care must be taken when simulating such an object numerically to place such an object away from a grid point.

### 3.2 ‘Glued’ Ansatze

### 3.2.1 The Three Region Ansatz

One ansatz for a defect-soliton system which we tried early on involved ‘glueing’ together three regions in an attempt to graft together a known ansatz for the soliton to a defect like object – see figure (2). In region I the field followed the

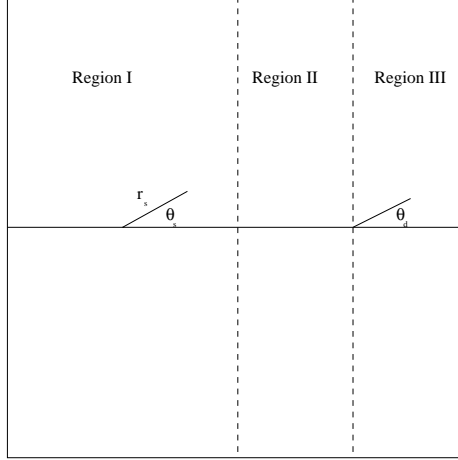


Figure 2: Regions and Coordinates for Glued Ansatz

standard lump ansatz for the  $O(3)$  sigma model. This is given by the hedgehog ansatz (10) with the profile function given by:

$$f(r) = \tan^{-1} \frac{2\lambda r}{1 - \lambda^2 r^2}, \quad (20)$$

where  $\lambda$  is an arbitrary (real) parameter describing the (inverse) ‘width’ of the lump. In region II the field is constant and equal to the vacuum value of region I – there should be little discrepancy at the border between regions I and II as a result, and any variation may be interpolated across several grid points in the simulation. In the region III the field is given by:

$$\vec{\phi} = \begin{pmatrix} \cos \theta_d \\ 0 \\ \sin \theta_d \end{pmatrix}, \quad (21)$$

for  $-\pi \leq \theta_d < \pi$ . The region II and region III fields match along the line  $\theta = \frac{\pi}{2}$  and, due to the identification  $\vec{\phi} \equiv -\vec{\phi}$ , along the line  $\theta = -\frac{\pi}{2}$ . This places a defect at the origin. Unfortunately this defect is far from stable – the energy of this defect is double that of the defect described by (17). Thus in the simulations of this total field configuration we have seen the emission of waves of radiation by the defect. These waves affected the skyrmion. To reduce these problems we have modified our ansatz as detailed below.

### 3.2.2 The Two Region Ansatz

We modified the above ansatz by replacing the field in regions II and III by the field below:

$$W = \tan \frac{\theta_d}{4} e^{-k(r_d - r_0)}, \quad (22)$$

where  $0 \leq \theta_d < 2\pi$  and  $W$  is the stereographic projection from the south pole. At a first glance this field looks as though it might tend to the vacuum value in all directions whilst looking like a defect at small radii. In fact, this is not the case – the field is smooth away from the origin, and therefore a loop around this field at infinity must be non-trivial. The field must vary dramatically as  $\theta$  approaches  $2\pi$  and  $r$  approaches infinity. We had hoped that this would not be a problem in the (finite) region of the simulation, but discretisation brought its own problems, as shown in figure (3). The line where  $W = 1$  must cross the last line of grid points on the large  $\theta_d$  side of the  $\theta_d = 0$  line. This leads to a point

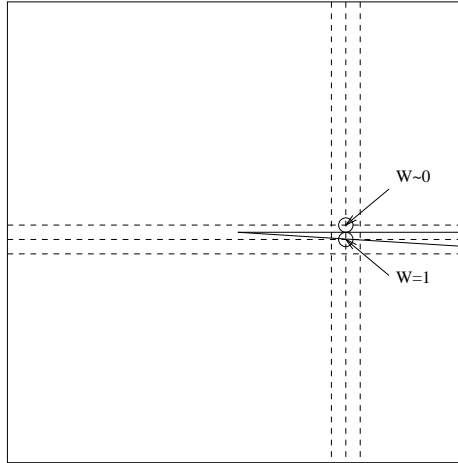


Figure 3: Diagram showing discretisation problem

where the variation in the field from one grid point to the next is as large as it can be, resulting in a region of high energy density. In fact this region also has defect type winding number – the ansatz has created a second defect in a far from equilibrium configuration. In fact if one constructs an ansatz which tends to constant field at spatial infinity (or the edge of the simulation region) then the space must contain an even number of defects. A loop at large  $r$  which maps to one point in  $\mathbb{RP}^2$  must correspond to the trivial element of  $\pi_2(\mathbb{RP}^2) = \mathbb{Z}_2$ , so the number of defects inside this loop must be even.

### 3.3 The Stereographic Defect - Soliton Ansatz

To create an ansatz for a field configuration including both a soliton and a defect we must re-express our field configurations using the stereographic map,  $W$ . A projection from the south pole causes the north pole,  $\phi_3 = 1$ , to map to  $W = 0$  and the south pole to map to  $W = \infty$ . Note that the antipodal identification under this map is given by

$$W \mapsto -\frac{1}{W^*}. \quad (23)$$

Our ansatz must a) look like a soliton near the soliton, b) look like a defect near the defect, c) look like a defect at infinity and d) be smooth at all points away from the defect.

A single soliton at the origin may be described by the field

$$\vec{\phi} = \begin{pmatrix} \alpha \cos(\theta - \gamma) \\ \alpha \sin(\theta - \gamma) \\ \beta \end{pmatrix}, \quad (24)$$

where  $\alpha = \frac{2\lambda r}{1+\lambda^2 r^2}$ ,  $\beta = \frac{1-\lambda^2 r^2}{1+\lambda^2 r^2}$ ,  $\gamma$  is an arbitrary (real) phase parameter,  $\lambda$  is an arbitrary (real) parameter characterising the width of the soliton, and  $(r, \theta)$  are polar coordinates. Note that this is the hedgehog ansatz with the profile function given by (20). To combine this with a defect we choose the point of projection of both fields such that the soliton at infinity maps to a number of modulus 1, and the line along which the defect field identifies approaches 0 from one side and  $\infty$  from the other. These fields are given below.

$$W_s = \frac{\alpha \sin(\theta - \gamma) + i\beta}{1 + \alpha \cos(\theta - \gamma)}, \quad (25)$$

$$\begin{aligned} W_d &= \frac{\sin(\frac{\theta}{2})}{1 + \cos(\frac{\theta}{2})} \\ &= \tan(\frac{\theta}{4}). \end{aligned} \quad (26)$$

If we multiply these fields we find

$$W_T = \frac{\alpha \sin(\theta_s - \gamma) + i\beta}{1 + \alpha \cos(\theta_s - \gamma)} \tan(\frac{\theta_d}{4}), \quad (27)$$

where  $\theta_d$  is the polar angle coordinate with respect to the position of the defect and  $(r, \theta_s)$  are the polar coordinates with respect to the position of the soliton. This ansatz obeys conditions c) and d) above. c) is satisfied as at infinity  $W_T = -i \times W_d$ . This is acceptable as multiplying a field configuration by a number of unit modulus is merely a rotation about the axis of projection. d) is also satisfied as the line of identification in  $W_d$  is preserved by the multiplication  $-0 \times W_s = 0$  and (crudely speaking)  $\infty \times W_s = \infty$ . Condition a) is fulfilled if the soliton and defect are sufficiently separated for the variation in  $W_d$  to be small across the scale of the soliton. Condition b), however, is only fulfilled if  $(\theta_s - \gamma) = (2n + 1)\frac{\pi}{2}$  where  $n \in \mathbb{Z}$ .

### 3.4 The Inhomogeneous Defect - Soliton Ansatz

An alternative ansatz involves using the inhomogeneous coordinates outlined in section (1.2). If we define a complex number

$$\mathcal{W} = \frac{\phi_1 + i\phi_2}{\phi_3} \quad (28)$$

then we can express the soliton field as a complex number which tends to 0 at  $r$  tends to 0 and  $\infty$ . If we add this to the defect field then the result must satisfy conditions c) and d) outlined in section (3.3). c) is satisfied because the map used is a map of  $\mathbb{R}P^2$ , not  $S^2$  and so needs no line of identification for the defect ansatz, whilst d) is obeyed as the soliton field vanishes at infinity, leaving only the defect field. Explicitly, the fields look like this:

$$\mathcal{W}_s = \frac{\alpha}{\beta} e^{i(\theta_s - \gamma)}, \quad (29)$$

$$\mathcal{W}_d = \tan\left(\frac{\theta_d}{2}\right), \quad (30)$$

$$\mathcal{W}_T = \frac{\alpha}{\beta} e^{i(\theta_s - \gamma)} + \tan\left(\frac{\theta_d}{2}\right). \quad (31)$$

This expression obeys a) if  $\mathcal{W}_d$  is small around the position of the soliton. Condition b) is only met if  $\mathcal{W}_s$  is small in the region of the defect, and in the example above condition b) is less well satisfied if  $\mathcal{W}_s$  has an imaginary component at the defect.

### 3.5 Simulation methods

For simulations of a defect-soliton system we introduced a conformal grid in a similar manner to Leese et al in [9]. This involved changing the physical coordinates  $(x, y)$  to  $(x', y')$  such that

$$X' = \frac{X}{1 + |X|}. \quad (32)$$

This allows a much larger area to be simulated. The grid was  $199 \times 199$  points with  $dX' = 0.01$ . This conformal grid was introduced to reduce boundary effects. Again, the timestep length was set to half the gridpoint spacing.

Another alteration to the simulation for defect-soliton systems was the introduction of a period of relaxation before the simulation was allowed to run freely.  $Q_{ij}$  was set to zero throughout the grid every 10 timesteps for the first 100 timesteps to take the simulation as close as possible to its minimal energy before the simulation proper began.

### 3.6 Results

The soliton-defect system displayed certain generic characteristics – a “spreading” channel and a “spiking” channel according to the phase of the soliton. In

the spreading channel the soliton would become broader and broader until it significantly overlapped the defect, at which point it would unwind, and the energy would be released to infinity as radiation. In the spiking channel the soliton would become more and more localised until the variation in the field became numerically untenable. The defect would remain stationary in all simulations, whilst the soliton would move only a very small distance, to the extent that variations in the width of the soliton would be far more significant than any movement of the maxima of the soliton.

### 3.6.1 Stereographic Ansatz

We used the stereographic ansatz (equation(27)) as our initial condition with  $\lambda = 2.5$ , and the initial soliton position relative to the defect at  $\theta_d = \pi$ ,  $r_d = 2.5$ . We shall discuss the results of simulations with  $\gamma$  set to  $\frac{\pi}{2}$ ,  $-\frac{\pi}{2}$ , 0 and  $-\frac{\pi}{4}$ . After the initial period of relaxation energy was conserved to better than 0.05% in all of these simulations. The period of relaxation ended at  $t = 0.5$ , after which the simulation ran freely until  $t = 9.995$ , unless the simulation became untenable due to soliton spiking.

When the simulation was run with the phase initially set to  $\gamma = -\frac{\pi}{2}$  the soliton became narrower with time as described above (see figure (5)). This resulted in the simulation ending at  $t = 3.745$ .

When  $\gamma = \frac{\pi}{2}$  the soliton spread out and eventually unwound as described above (see figure (4)). When  $\gamma = 0$  was simulated the soliton was still subject to spreading and unwinding – the spreading channel is wider than the spiking channel.

For  $\gamma = -\frac{\pi}{4}$  the soliton began to spike, but after a period of time the the rate of spiking slowed and the soliton began to spread, with the soliton eventually unwinding (see figure(6)). This also suggests that the spiking channel is unstable.

Table (1) shows the energies of various simulations with initial conditions given by this ansatz. Note that these energies depend heavily on the lattice spacing at the defect, and are therefore only of value when comparing the different channels.

$\gamma$	Initial Energy ( $t = 0$ )	Energy after Relaxation ( $t = 0.5$ )	Time at end of Simulation	Final Energy
$\frac{\pi}{2}$	1.439	1.435	9.995	1.435
0	1.520	1.512	9.995	1.512
$-\frac{\pi}{2}$	1.595	1.590	3.745	1.591

Table 1: Energy of System in Stereographic Ansatz

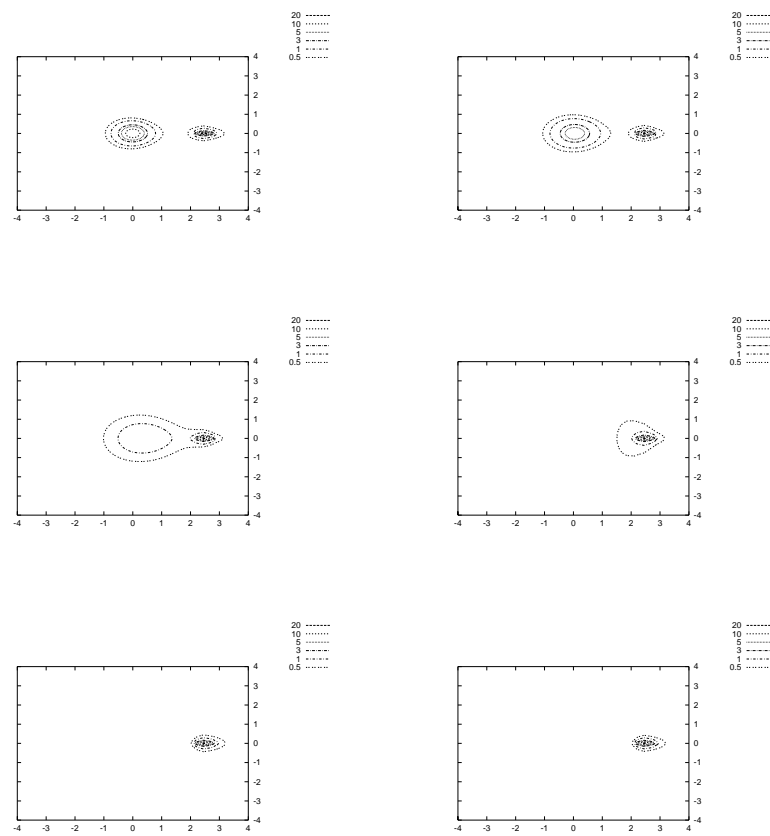


Figure 4: Energy density for  $\gamma = \frac{\pi}{2}$  at  $t=0, 2, 4, 6, 8$  and  $9.975$

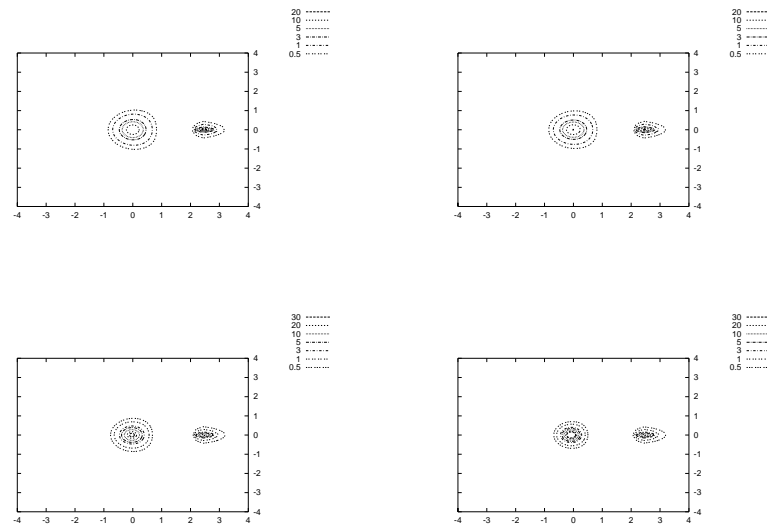


Figure 5: Energy density for  $\gamma = -\frac{\pi}{2}$  at  $t=0, 1, 2$  and  $3$

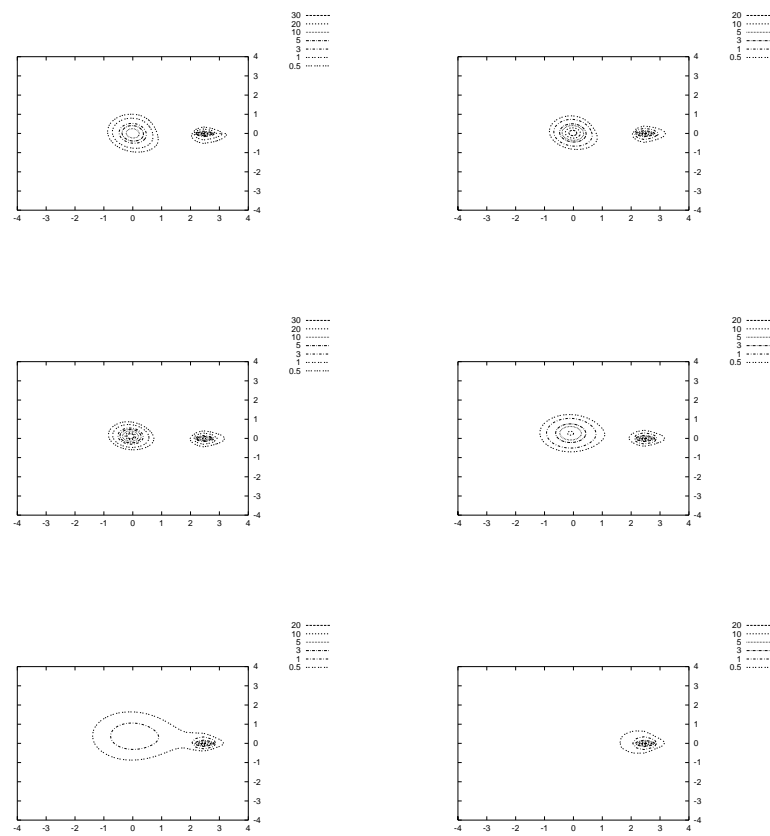


Figure 6: Energy density for  $\gamma = -\frac{\pi}{4}$  at  $t=0, 2, 4, 6, 8$  and  $9.75$

### 3.6.2 Inhomogeneous Ansatz

We also simulated the soliton defect system using the inhomogeneous ansatz (equation (31)) as the initial condition, with the initial  $\lambda = 2.5$ , and the initial soliton position relative to the defect at  $\theta_d = 0$ ,  $r_d = 2.5$ , so that the contribution to the ansatz from the soliton is significant compared to that from the defect in the region of the soliton. With this ansatz the soliton spikes for  $\gamma = \frac{\pi}{2}$  (see figure (8)) and spreads at  $\gamma = -\frac{\pi}{2}$  (see figure (7)). If  $\gamma = \frac{\pi}{4}$  in the initial condition, the soliton starts to spike, but then later spreads (see figure(9)). Table (2) shows the energies for simulations with these initial conditions. Again, these energies are only included for their value in comparing channels and to show that energy is conserved during the free run of the simulation.

$\gamma$	Initial Energy ( $t = 0$ )	Energy after Relaxation ( $t = 0.5$ )	Time at end of Simulation	Final Energy
$\frac{\pi}{2}$	1.597	1.593	3.745	1.593
0	1.523	1.516	9.995	1.516
$-\frac{\pi}{2}$	1.442	1.437	9.995	1.438

Table 2: Energy of System in Inhomogeneous Ansatz

### 3.7 Collective Coordinate Approach

To further the understanding of our numerical results we carried out some approximate analytic work based on the so called collective coordinate approach. We substituted one of our ansatze into the Lagrangian density, integrated over the spatial variables to find a true Lagrangian and then considered one or more of the ansatz parameters as dynamic variables, so for example Lagrangian (1) together with

$$\vec{\phi} = \vec{\phi}(\lambda, \dot{\lambda}, x, y), \quad (33)$$

implies that

$$\mathcal{L} = \mathcal{L}(\lambda, \dot{\lambda}, x, y), \quad (34)$$

which may then be integrated over to give

$$L = \int \mathcal{L}(\lambda, \dot{\lambda}, x, y) dx dy = L(\lambda, \dot{\lambda}), \quad (35)$$

allowing us to construct an equation of motion for  $\lambda$ .

This effectively constrains the solutions of the field theory to the submanifold defined by the ansatz – in the example above our solutions are constrained to a 2 dimensional submanifold of the infinite dimensional phase space of  $\vec{\phi}(x, y)$ . This does not allow for soliton unwinding or the release of radiation with our ansatze, as the ansatze never have radiation and always have a soliton.

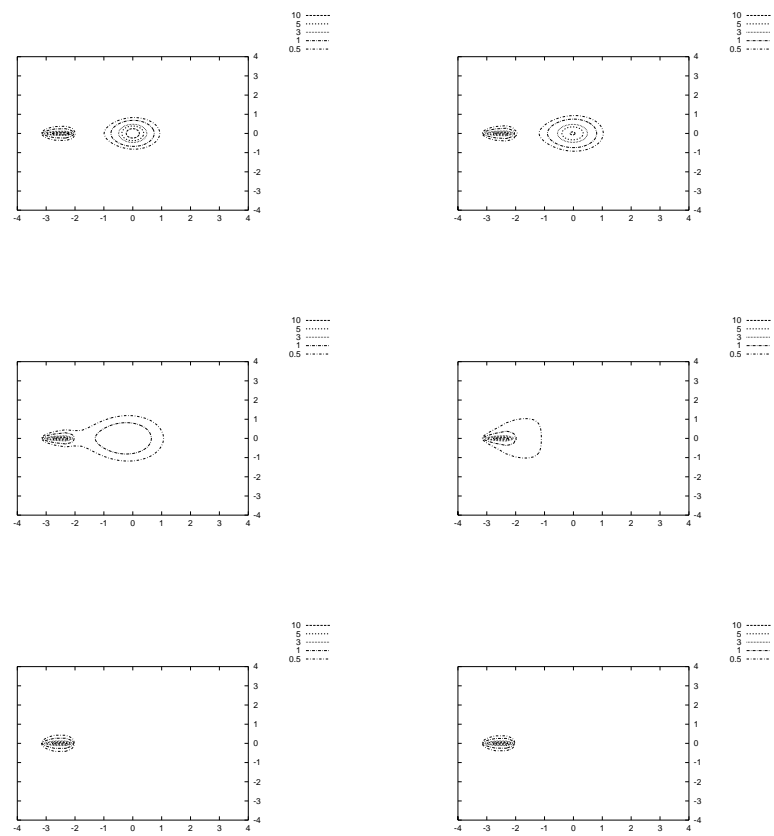


Figure 7: Energy density for  $\gamma = -\frac{\pi}{2}$  at  $t=0, 2, 4, 6, 8$  and  $9.975$

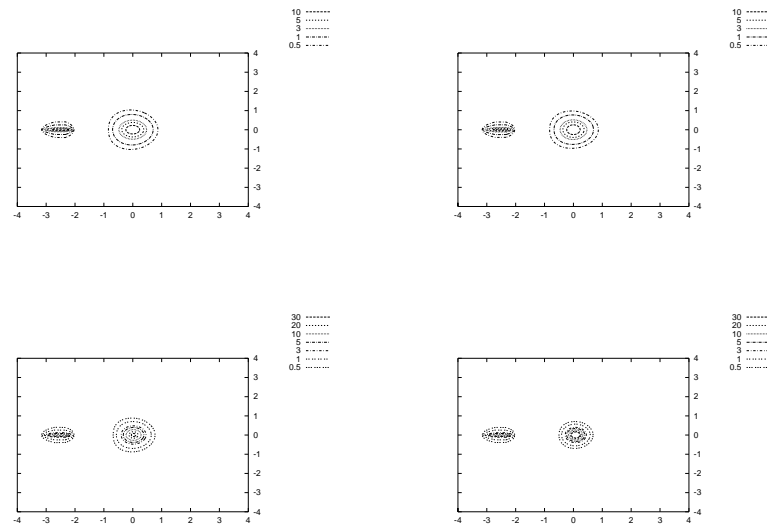


Figure 8: Energy density for  $\gamma = \frac{\pi}{2}$  at  $t=0, 1, 2$  and  $3$

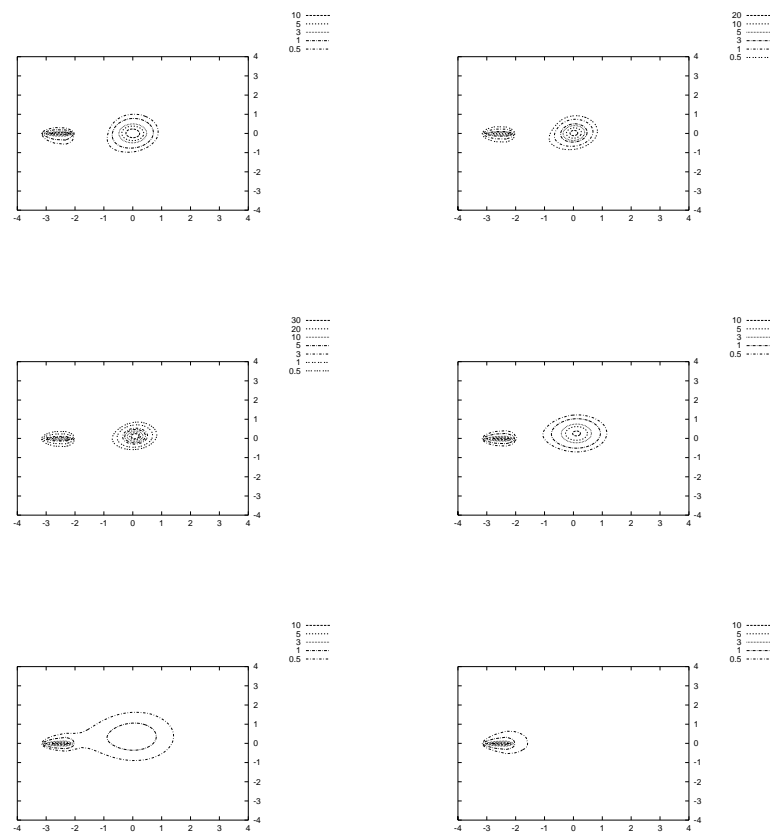


Figure 9: Energy density for  $\gamma = \frac{\pi}{4}$  at  $t=0, 2, 4, 6, 8$  and  $9.75$

If we take the ansatz (27) together with the Lagrangian (1) expressed in terms of stereographic coordinates

$$\mathcal{L} = \frac{\partial_\mu W \partial^\mu W^*}{4(1 + |W|^2)^2}, \quad (36)$$

we may construct the Lagrangian density in terms of position and a few parameters. If we take the initial soliton and defect position outlined in section (3.6.1) then  $W$  becomes

$$W = \frac{2\lambda(r \sin(\theta - \gamma) - 2.5 \sin \gamma) + i(1 - \lambda^2(r^2 + 5r \cos \theta + 6.25))}{1 + \lambda^2(r^2 + 5r \cos \theta + 6.25) + 2\lambda(r \cos(\theta - \gamma) + 2.5 \cos \gamma)} \tan \frac{\theta}{4}, \quad (37)$$

where  $(r, \theta)$  are polar coordinates,  $\lambda$  parameterises the (inverse) width of the soliton and  $\gamma$  is the phase of the soliton. Note that the soliton has position  $(2.5, \pi)$  and the defect is at the origin in this coordinate system. Taking spatial derivatives of  $W$  is then a straight forward if somewhat tedious process. Time derivatives may be found by treating one or more of the parameters as dynamic - if we consider  $\lambda$  to be dynamic and the other parameters to be static the  $\partial_t = \dot{\lambda} \partial_\lambda$ . This substitution of an ansatz and use of parameters as dynamic variables is equivalent to assuming that the field configuration moves quasi-statically from one configuration to another with different values of the dynamic variables. This assumption is valid only if our ansatz is close to equilibrium and our dynamic parameter only varies slowly with time (i.e. in this case  $\dot{\lambda}$  is small).

Using this approximation our Lagrangian density becomes

$$\mathcal{L} = \frac{r^2 \partial_r W \partial_r W^* + \partial_\theta W \partial_\theta W^* - r^2 \dot{\lambda}^2 \partial_\lambda W \partial_\lambda W^*}{4r^2(1 + |W|^2)^2}. \quad (38)$$

So our approximate Lagrangian with a time dependant  $\lambda$  becomes

$$L = A(\lambda) - \dot{\lambda}^2 B(\lambda), \quad (39)$$

where

$$A(\lambda) = \int \frac{r^2 \partial_r W \partial_r W^* + \partial_\theta W \partial_\theta W^*}{4r^2(1 + |W|^2)^2} r dr d\theta \quad (40)$$

and

$$B(\lambda) = \int \frac{\partial_\lambda W \partial_\lambda W^*}{4(1 + |W|^2)^2} r dr d\theta. \quad (41)$$

The Euler-Lagrange equation then gives us

$$\ddot{\lambda} = \frac{-(A'(\lambda) + \dot{\lambda}^2 B'(\lambda))}{2B(\lambda)}. \quad (42)$$

We considered the example above, where all variables are static except for  $\lambda$ , but found an analytic integration to be intractable. We carried out the

integration and time evolution numerically, using a fourth order Runge-Kutta algorithm for the time evolution. We also carried out a similar analysis using the inhomogeneous ansatz (31).

In figures (10, 11) we show the results of this treatment against those of the full simulation. The two treatments produce broadly similar results, although the rapidity of the broadening and spiking is faster in the full simulation. This is not entirely unreasonable considering that we have moved from around 160,000 degrees of freedom to 2! The curves from the full simulation were found by finding the maximum winding number density on the grid and then finding the value of  $\lambda$  that would give a single soliton of the form of equation (24) this maximum winding number density. One consequence of this technique is that for broad solitons the maximum winding number for the soliton may be smaller than the maximum on the grid – this leads to the curves for the broadening channel becoming unreliable at around  $t = 5$ . Naturally, the collective coordinate simulation began at the point when the relaxation ended in the full simulation.

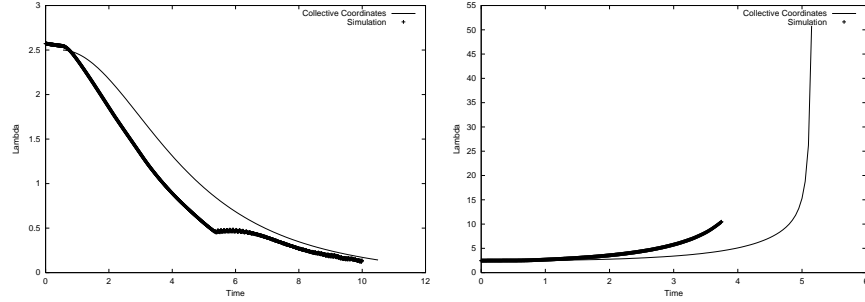


Figure 10:  $\lambda$  vs. time for spiking and broadening channels in the stereographic ansatz

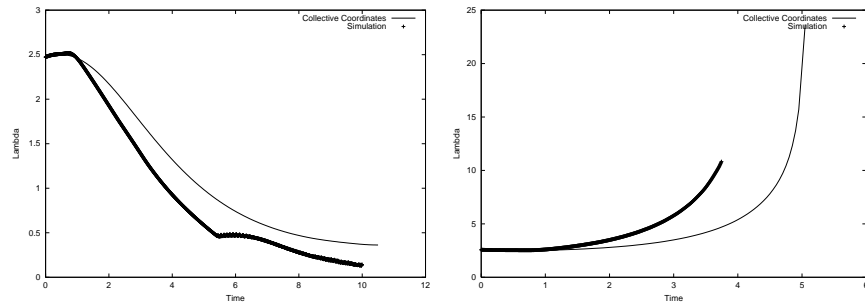


Figure 11:  $\lambda$  vs. time for spiking and broadening channels in the inhomogeneous ansatz

## 4 Conclusions

We have examined the sigma model and baby Skyrme model with  $\mathbb{R}P^2$  as a target space and found these models to be identical to their  $S^2$  counterparts in the absence of defects. We examined the interaction between defects and soliton-like lumps in the sigma model and found the interaction to depend on the relative phase of the lump. We found a channel which causes the soliton to broaden and another which causes the soliton to spike. When the soliton overlapped the defect significantly, the soliton would unwind. We broadly reproduced this behaviour with the collective coordinate approach, using only two collective coordinates.

A range of possibilities for future work present themselves – studying the interaction between two defects, the interactions of two lumps in the presence of a defect and the behaviour of the  $\mathbb{R}P^2$  sigma model on a torus all have the potential to exhibit new and interesting behaviour.

## Acknowledgements

I would like to thank Wojtek Zakrzewski for his advice and guidance. I would also like to thank PPARC for funding this research.

## References

- [1] Skyrme THR (1961) A Nonlinear Field Theory, *Proc. R. Soc. A* **260** 127-38
- [2] Piette BMAG and Zakrzewski WJ (1995) Skyrmion Dynamics in (2 + 1) Dimensions, *Chaos, Solitons and Fractals* **5** 2495-508
- [3] Weidig T (1999) The Baby Skyrme Models and their Multi-Skyrmions, *Nonlinearity* **12** 1489-1503
- [4] Croom FH, Basic Concepts of Algebraic Topology (New York: Springer Verlay (1978))
- [5] Trebin H-R (1982) The Topology of Non-uniform Media in Condensed Matter Physics, *Adv. in Phys.* **31** 3 195-254
- [6] Piette BMAG and Zakrzewski WJ (1998) Numerical Integration of (2+1) Dimensional PDEs for  $S^2$  Valued Functions, *J. Comp. Phys.* **145** 359-81
- [7] Fadeev L and Niemi AJ (1997) Stable Knot-like Structures in Classical Field Theory *Nature* **387** 58 - 61
- [8] Battye RA and Sutcliffe PM (1998) To be or knot to be?, hep-th/9808129
- [9] Leese RA, Peyrard M and Zakrzewski WJ (1990) Soliton Stability in the  $O(3)$   $\sigma$ -model in (2+1) Dimensions, *Nonlinearity* **3** 387-412